Data-driven LPV Control for Disturbance Rejection in a Hybrid Isolation Platform

Elias Klauser, and Alireza Karimi

***Abstract*—A novel approach for linear parameter-varying (LPV) controller synthesis for adaptive rejection of frequency-varying sinusoidal disturbances is proposed. Only the frequency response data of a linear time-invariant (LTI) multiple-input multiple-output (MIMO) system is used to design the LPV controller that stabilizes the system for arbitrarily fast variation of the disturbance frequencies. Global stability is achieved thanks to the specific structure of the LPV controller and the use of integral quadratic constraints (IQC) to represent the frequency variations. The LPV controller is designed by convex optimization in the frequency domain. For experimental validation of the proposed method, a hybrid micro-vibration damping platform for space applications is considered. An LPV controller for rejection of unknown frequency-varying sinusoidal disturbances is designed and implemented on the real system. Experimental results demonstrate the effectiveness of the proposed approach in asymptotically rejecting disturbances and ensuring closed-loop stability against arbitrarily fast variations in disturbance frequencies.**

***Index Terms*—Data-driven control, Adaptive control, Linear parameter-varying systems, Convex optimization, Frequency-domain identification for control.**

I. Introduction

Disturbance rejection is a very important task in control design, as noise or external perturbations can significantly degrade the control performance. Numerous applications such as active suspension systems [1], optical stabilisation [2], control of robotic systems [3], vibration suppression in machinery [4] and active noise canceling systems [5], [6] rely on an effective disturbance rejection control. Oftentimes, the perturbation signals in such systems are periodic and can be represented as a sum of sinusoidal signals.

In such cases when the disturbance model is known a priori, control design based on the internal model principle (IMP) can be applied. An adaptive IMP- and model-based control design can be implemented using an observer to estimate the states of the disturbance model. These estimated states can then be used to adaptively reject a harmonic disturbance [7], [8]. Alternatively, the disturbance can be modeled as a linear parameter-varying (LPV) system in a linear fractional representation (LFR) [6]. The frequency variation of the sinusoidal disturbance is captured by the scheduling parameter of the LPV model, while the same scheduling parameter is used for the adaptation of an LPV controller. A collection of different approaches to a benchmark on adaptive rejection of unknown and time-varying multiple narrow band disturbances can be found in [9]. An active suspension system composed of a passive damper, an inertial actuator, a shaker, a transducer and an integrated controller is used for the study. The goal is to achieve rejection of multiple narrow-band sinusoidal disturbances without measuring them by using a feedback approach. As the disturbance signal is unknown, it must be estimated for controller adaptation. The authors in [10] propose an inverse plant model approximation. The compensation signal is generated by applying the estimated disturbance signal to the inverse plant model. An indirect adaptation approach is presented in [11] where a fixed-order H_∞ gain-scheduled controller is designed using convex optimization methods. This LPV controller, designed based on frequency-domain data, uses the estimated disturbance harmonics as scheduling signals for disturbance rejection. The case of adaptive rejection of unknown narrow-band disturbances in the presence of uncertain plants is treated in [12]. A dual Youla-Kuçera parametrization is used to incorporate the description of the plant model uncertainties by expressing a relation between the nominal and the uncertain plant. These model-based approaches require the availability of an accurate parametric plant model that must otherwise be identified. This system identification step can be very time-consuming and therefore costly, especially for complex systems.

For that reason, data-driven control design techniques are becoming increasingly attractive for industrial applications thanks to recent technological developments leading to higher computational power and improved sensor technologies. These techniques can directly minimize a control criterion based on measured input-output data, making them particularly advantageous in cases where a parametric plant model is unavailable or is difficult to identify. Frequency response data can effectively be used for the analysis and synthesis of linear control systems, as it can be easily computed from input-output data avoiding any modelling error. Such methods are widely used in industry, as demonstrated by the classic loop shaping technique. As most control performance and robust stability conditions can be represented in the frequency domain, new data-driven methods that employ only frequency-domain data and convex optimisation programming to compute robust controllers have been proposed in the literature. A fixed-structure data-driven controller design method for multivariable systems with mixed $\mathcal{H}_2/\mathcal{H}_\infty$ sensitivity performance is proposed in [13] and applied to passivity-based controller design [14] and distributed control of microgrids [15]. This approach can be extended to linear parameter-varying (LPV) control design

*This work is funded by the European Space Agency ESA Contract No. 4000133258/20/NL/MH/hm.

E. Klauser is with CSEM SA, Rue Jaquet-Droz 1, CH-2002 Neuchâtel, Switzerland, and also with the Laboratoire d'Automatique, École Polytechnique Fédérale de Lausanne, CH-1015 Lausanne, Switzerland (e-mail: elias.klauser@csem.ch)

A. Karimi is with the Laboratoire d'Automatique, École Polytechnique Fédérale de Lausanne, CH-1015 Lausanne, Switzerland (e-mail: alireza.karimi@epfl.ch)

by gridding the scheduling parameter vector using a fixed number of operating points [16]. A similar approach is applied to a Cartesian robot with nonlinear dynamics for position-dependent control in [17]. A frequency-domain gain-scheduled control design for rejection of time-varying narrow-band disturbances is presented in [11]. All of these methods consider control design constraints at frozen operating points and do not strictly guarantee stability for the time-varying nature of the scheduling parameters. Intrinsic stability guarantees for arbitrarily fast variation of scheduling parameters have been proposed for model-based approaches [6] and are missing in the state of the art of data-driven methods.

The Integral Quadratic Constraints (IQC) framework, introduced in [18], provides a flexible mathematical approach for the representation and analysis of various forms of nonlinearities and uncertainties, including parametric uncertainties, time-varying parameter, time-delays, and norm and sector bounded nonlinearities. This framework can be used to establish sufficient stability conditions in frequency domain and to analyze systems with multiple uncertainty types using a single composite IQC. Various techniques have been developed for model-based robust control analysis and synthesis using IQC framework [19], [20], including a MATLAB toolbox [21]. However, in the data-driven context, there are limited results. A necessary and sufficient condition has been developed for a linear time-invariant (LTI) system to satisfy a given IQC using single input-output trajectory of finite length [22]. Data-driven methods that combine robust stability and performance analysis in an IQC-based optimisation have been explored for designing MIMO linear parameter-varying (LPV) controllers directly from frequency-domain data [23]. This method is employed for LPV controller design of control moment gyroscopes (CMG) in [24]. Note again that all the presented LPV control design approaches provide only local stability guarantees for frozen dynamics at selected operating points. Stability guarantees for the variation of the scheduling parameter are not strictly provided.

In this paper, the objective is to synthesize a control system that can effectively reject unknown frequency-varying sinusoidal disturbances while ensuring closed-loop stability. This is achieved using only the frequency-domain data obtained from the LTI plant model and no parametric model is required. The control system consists of three main components: an online disturbance frequency estimator, an LPV controller with a scheduling parameter as a function of the estimated disturbance frequency, and an LTI controller. The LPV control part is designed to asymptotically reject the sinusoidal disturbances. Meanwhile, the LTI controller is designed to guarantee closed-loop stability, even in the presence of rapid variations in the estimated frequency within the LPV controller. The main idea is to augment the LTI plant model with the LPV controller in the frequency domain and pull out the scheduling parameter as a time-varying uncertainty. Then, the IQC formalism is used to compute an LTI controller for the augmented LPV plant which stabilizes the closed-loop system for the arbitrarily fast variation of the scheduling parameter. A novel linear matrix inequality (LMI) based on the IQC framework is presented allowing to guarantee stability for a bounded interval of the scheduling parameter. In addition, a significant reduction of computational complexity over current data-driven methods (e.g. [17], [23]) is achieved as no gridding of the scheduling parameter vector is required.

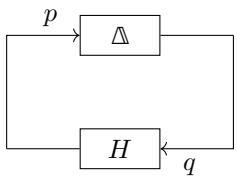

Fig. 1. Basic feedback configuration

The remainder of the paper is organised as follows: First, the notations, the basic problem, the IQC formalism and a general frequency-domain control synthesis for LFT systems are introduced (Section II). Then, an iterative LPV control design algorithm for single- and multi-harmonic rejection is presented using an IQC-based LMI constraint (Section III). The resulting controller guarantees stability for arbitrarily fast variation of the scheduling parameters lying in a bounded interval. Finally, the proposed method is used to design an adaptive control scheme for a hybrid active-passive micro-vibration damping platform (MIVIDA) with the goal of adaptively rejecting unknown external perturbations (Section IV). The MIVIDA is a demonstrator for a spaceborne system that was designed to actively isolate a sensitive payload from vibrations present on board the spacecraft.

II. Preliminaries

Notations: The set of real rational stable transfer functions with bounded infinity norm is denoted by $\mathcal{RH}_\infty$. $A \succ (\succeq)\, B$ indicates that $A - B$ is a positive (semi-) definite matrix and $A \prec (\preceq)\, B$ indicates $A - B$ is negative (semi-) definite. The zero and identity matrices of appropriate size are denoted 0 and I respectively. The transpose of a matrix A is denoted by A^T and its conjugate transpose by A^*. Right inverse of A is denoted as $A^{\mathsf{R}} := A^*(AA^*)^{-1}$, and its left inverse is denoted as $A^{\mathsf{L}} := (A^*A)^{-1}A^*$.

A. Integral Quadratic Constraints

In the developments that follow, only discrete-time systems are considered. Two discrete-time signals p and q are said to satisfy the IQC defined by a multiplier Π, if

$$\int_\Omega \begin{bmatrix} P(e^{j\omega}) \\ Q(e^{j\omega}) \end{bmatrix}^* \Pi(e^{j\omega}) \begin{bmatrix} P(e^{j\omega}) \\ Q(e^{j\omega}) \end{bmatrix} d\omega \geq 0 \qquad (1)$$

where $P(e^{j\omega})$ and $Q(e^{j\omega})$ are the Fourier transform of the signals p and q respectively and $\Omega := [-\pi/T_s, \pi/T_s)$ with the sampling time T_s [19]. From [18, Theorem 1], the feedback connection between $H \in \mathcal{RH}_\infty$ and a bounded causal operator $\mathbb{\Delta}$ (see Fig. 1) is stable if,

1) the interconnection of H and $\tau\mathbb{\Delta}$ is well-posed for all $\tau \in [0, 1]$;
2) $\tau\mathbb{\Delta}$ satisfies the IQC defined by Π for all $\tau \in [0, 1]$;

3) The following inequality is satisfied:

$$\begin{bmatrix} H(e^{j\omega}) \\ I \end{bmatrix}^* \Pi(e^{j\omega}) \begin{bmatrix} H(e^{j\omega}) \\ I \end{bmatrix} \prec 0 \qquad \forall \omega \in \Omega \quad (2)$$

Remark 1: If the upper left corner of Π is positive semi-definite and the lower right corner is negative semi-definite, then using [18, Remark 2], $\tau\mathbb{\Delta}$ satisfies the IQC defined by Π for all $\tau \in [0, 1]$ if and only if $\mathbb{\Delta}$ satisfies the IQC.

Numerous forms of multiplier matrices Π for different uncertainty types have been proposed in literature. For arbitrarily fast time-varying scalar uncertainties, i.e. $\mathbb{\Delta}(k) = \delta(k)I$, $|\delta(k)| \leq \eta, \forall k \in \mathbb{R}_+$, a stationary multiplier Π can be defined as [25]:

$$\Pi = \begin{pmatrix} \eta^2 D & E \\ E^T & -D \end{pmatrix}, \quad (3)$$

where $D = D^T \succeq 0,\ E = -E^T$.

A system analysis step can be performed using (2) to find a multiplier matrix Π which satisfies the constraint. From (3), the upper bound η on $|\delta(k)|$ can be identified allowing to compute bounds on the uncertainty block $\mathbb{\Delta}(k)$. Similarly, the obtained IQC can be used as a control design constraint to guarantee robustness for a desired fixed upper bound η.

B. Basic problem statement

The system to be controlled is a multivariable linear time-invariant (LTI-MIMO) plant P_2 referred to as secondary path with n_u input channels and n_y output channels. The FRF matrix can be acquired from classical system identification experiments [26]. Given n_u sets of finite sampled input/output data which can be acquired from n_u open-loop identification experiments, the corresponding discrete-time FRF can be estimated as:

$$P_2(e^{j\omega}) = \left[\sum_{k=0}^{M-1} \mathbb{Y}(k) e^{-j\omega T_s k}\right] \left[\sum_{k=0}^{M-1} \mathbb{U}(k) e^{-j\omega T_s k}\right]^{-1} \quad (4)$$

where M is the number of data points and each column of $\mathbb{U}(k)$ and $\mathbb{Y}(k)$ represents respectively the inputs and outputs at the time sample k at one experiment. It is assumed that $P_2(e^{j\omega})$ is bounded for all frequencies $\omega \in \Omega$. The estimation errors can be considered as model uncertainty and taken into account for the controller design, however, they are neglected to focus on the main subject of this paper. In addition, an LTI perturbation model $P_1(e^{j\omega})$ representative of the primary path can be used to model the propagation of an exogenous perturbation signal d to the measurement y (see Fig. 3). For the presented control method, the disturbance signal d is supposed to contain sinusoidal components with an unknown time-varying harmonic frequency $\rho(k)$. The variation of the frequency can be large and fast but occurs seldom. The control objective is to asymptotically reject this disturbance.

C. Control design for LFT systems

A method to design fixed-structure frequency-domain controller based on linear fractional transform (LFT) representation is presented in [27]. A convex optimisation problem using LMIs is proposed to obtain an LTI controller with a fixed-structure parametrization. Since this method will be used in this paper, a summary of the main result is given in this section.

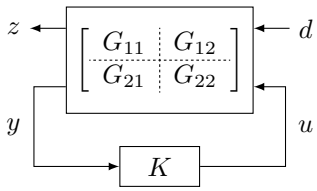

Fig. 2. LFT interconnection between generalized system and controller

The FRF of a generalized system G with exogenous signals $d \in \mathbb{R}^{n_d}$, control inputs $u \in \mathbb{R}^{n_u}$, measurements $y \in \mathbb{R}^{n_y}$ and performance channels $z \in \mathbb{R}^{n_z}$ can be presented as:

$$\begin{bmatrix} z \\ y \end{bmatrix} = \left[\begin{array}{c:c} G_{11} & G_{12} \\ \hdashline G_{21} & G_{22} \end{array}\right] \begin{bmatrix} d \\ u \end{bmatrix}.$$

The aim is to design an LTI controller K in order to compensate for the effect of the exogenous disturbances d on the performance channels z. The corresponding LFT represented in Fig. 2 is given by

$$\mathcal{F}_l(G, K) = T_{zd} = G_{11} + G_{12}K(I - G_{22}K)^{-1}G_{21}. \quad (5)$$

Assuming the closed-loop system is stable, the infinity norm of T_{zd} can be expressed as

$$||T_{zd}||_\infty^2 = \sup_{\omega \in \Omega} \bar{\sigma}(T_{zd}^*(e^{j\omega}) T_{zd}(e^{j\omega}))$$

where $\bar{\sigma}$ is the maximum singular value. This can be evaluated if $G(e^{j\omega})$, the FRF of $\mathcal{G}$, $\forall \omega \in \Omega$ is available. As an example, an $\mathcal{H}_\infty$ control design problem can be formulated as the minimization of the spectral norm:

$$\begin{aligned} &\min_{K,\gamma} \gamma \\ &\text{s.t.} \quad T_{zd}^*(e^{j\omega}) T_{zd}(e^{j\omega}) \preceq \gamma I, \qquad \forall \omega \in \Omega \end{aligned} \quad (6)$$

The controller K can be parameterized as $K = Y^{-1}X$, where X and Y are both $\mathcal{RH}_\infty$ matrix transfer functions linear in optimization variables. Assuming that G_{12} is full column rank $\forall \omega \in \Omega$, we can define

$$\Phi = (Y - XG_{22})\, G_{12}^{\mathsf{L}},$$

as a linear function of the optimization variables. Then, T_{zd} can be expressed as

$$T_{zd} \quad = \Phi^{\mathsf{R}} (\Phi G_{11} + XG_{21}) + \Psi G_{11} \quad (7)$$

where $\Psi = I - \Phi^{\mathsf{R}}\Phi = I - G_{12}G_{12}^{\mathsf{L}}$. The constraint from (6) can now be reformulated as,

$$\begin{aligned} T_{zd}^* T_{zd} = &(\Phi G_{11} + XG_{21})^* (\Phi\Phi^*)^{-1} (\Phi G_{11} + XG_{21}) \\ &+ (\Psi G_{11})^* (\Psi G_{11}) \prec \gamma I \end{aligned} \quad (8)$$

using the fact that $\Psi^*\Phi^{\mathsf{R}} = \Psi\Phi^{\mathsf{R}} = \Phi^{\mathsf{R}} - \Phi^{\mathsf{R}}\Phi\Phi^{\mathsf{R}} = 0$ and $(\Phi\Phi^*)^{\mathsf{R}} = (\Phi\Phi^*)^{-1}$. Using the Schur complement lemma, (8) can be expressed as

$$\begin{bmatrix} \gamma I - \Lambda & (\Phi G_{11} + XG_{21})^* \\ (\Phi G_{11} + XG_{21}) & \Phi\Phi^* \end{bmatrix} \succ 0, \quad (9)$$

where $\Lambda = (\Psi G_{11})^*(\Psi G_{11})$. This constraint is not convex and does not guarantee the closed-loop stability. It is shown in [27] that a convex lower bound on the quadratic term $\Phi\Phi^*$ can be obtained that ensures the closed-loop stability as well:

$$\Phi\Phi^* \succeq \Phi\Phi_c^* + \Phi_c\Phi^* - \Phi_c\Phi_c^* \tag{10}$$

where $\Phi_c = (Y_c - X_c G_{22})\, G_{12}^{\mathsf{L}}$, and $K_c = Y_c^{-1}X_c$ is an initial stabilizing controller. In practice, $K_c = 0$ for open-loop stable systems. The optimisation problem (6) can now be formulated as:

$$\begin{aligned} &\min_{X,Y} \gamma \\ &\begin{bmatrix} \gamma I - \Lambda & (\Phi G_{11} + X G_{21})^* \\ \star & \Phi\Phi_c^* + \Phi_c\Phi^* - \Phi_c\Phi_c^* \end{bmatrix}(e^{j\omega}) \succ 0 \quad \forall \omega \in \Omega, \end{aligned} \tag{11}$$

To solve the optimisation problem, a grid-based approach can be employed. The results can be improved using an iterative approach where the controller K is used as the initial stabilising control for the next iteration. This sequence of convex optimisation problems converges to a local optimal solution of the original nonlinear problem. For a more detailed explanation of the method, refer to [27].

III. Main Results

A. Controller structure for single harmonic rejection

Due to the time-varying nature of the disturbance frequency, P_2 shall be controlled by an LPV controller. We choose the LPV controller as the multiplication of an LTI controller $K(z)$ and a time-varying filter $N(z,\theta(k))$:

$$K_N(z,\theta(k)) = K(z)N(z,\theta(k)),$$

where $\theta(k) \in \Theta$ is the scheduling parameter. The control system architecture is schematically presented in Fig. 3. A time-varying filter $N(z,\theta(k))$ for a fixed value of $\theta(k) = \theta_c$ ensures asymptotic performance for disturbance rejection. In accordance with the IMP, $N(z,\theta_c)$ is chosen as an approximation of the z-transform of a sinusoidal signal. Hence, in the steady-state case with θ_c constant, disturbance rejection is achieved based on the IMP. The scheduling parameter $\theta(k)$ is chosen such that $\theta(k) = -2\cos(T_s\rho(k))$ where $\rho(k)$ is the time-varying frequency of the sinusoidal disturbance. The scheduling parameter can be defined around a fixed frequency $\bar{\theta}$ as $\theta(k) = \bar{\theta} + \delta\theta(k)$ with $|\delta\theta(k)| \leq \eta$ such that $[\theta_{\min}, \theta_{\max}] = [\bar{\theta} - \eta, \bar{\theta} + \eta]$. A sliding discrete Fourier transform (SDFT) is used for the estimation of the unknown harmonic disturbance frequency $\rho(k)$ (see Section IV-B). The objective is to guarantee the closed-loop stability for fast variations of the estimated value. For a fixed stationary value of the scheduling parameter $\theta_c = \bar{\theta} + \delta\theta_c$, $N(z,\theta_c)$ can be defined as:

$$\begin{aligned} N(z,\theta_c) &= \frac{1}{1 + \beta(\bar{\theta} + \delta\theta_c)z^{-1} + \beta^2 z^{-2}} \\ &= \frac{\frac{1}{1+\beta\bar{\theta}z^{-1}+\beta^2z^{-2}}}{1 + \frac{\beta z^{-1}}{1+\beta\bar{\theta}z^{-1}+\beta^2z^{-2}}\delta\theta_c} = \frac{N(z,\bar{\theta})}{1 + \beta z^{-1}N(z,\bar{\theta})\delta\theta_c}, \end{aligned} \tag{12}$$

where β is a scalar factor allowing to adjust the damping of the resonance frequency according to the desired attenuation performance. As shown in (12), $N(z,\theta_c)$ can be represented as a feedback loop with $N(z,\bar{\theta})$ in the forward path and $\beta z^{-1}\delta\theta_c$ in the feedback. Then $\delta\theta_c$ can be pulled out as an uncertainty block in an LFR as $\mathcal{F}_l(\mathcal{N}_c, \delta\theta_c)$, where

$$\mathcal{N}_c = \begin{pmatrix} N(z,\bar{\theta}) & -N(z,\bar{\theta}) \\ \beta z^{-1}N(z,\bar{\theta}) & -\beta z^{-1}N(z,\bar{\theta}) \end{pmatrix}$$

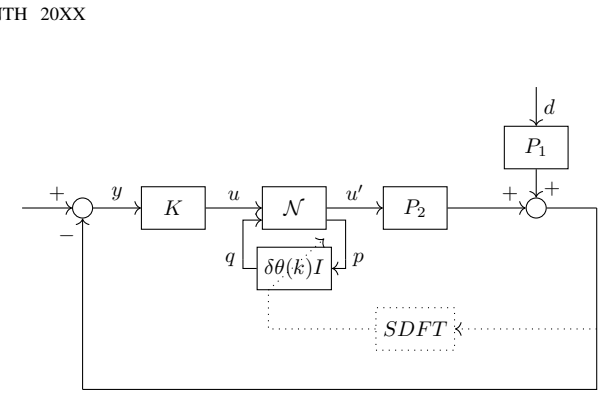

Fig. 3. Control system architecture with LTI controller part

For time-varying scheduling parameter in a multivariable system, $\delta\theta_c$ can be replaced with $\delta\theta(k)I$ and the LPV part of the control system can be defined by $\mathcal{F}_l(\mathcal{N}, \delta\theta(k)I)$ (see Fig. 3):

$$\begin{aligned} \begin{pmatrix} u' \\ p \end{pmatrix} &= \begin{pmatrix} \mathcal{N}_{11} & \mathcal{N}_{12} \\ \mathcal{N}_{21} & \mathcal{N}_{22} \end{pmatrix}\begin{pmatrix} u \\ q \end{pmatrix} \\ &= \begin{pmatrix} N(z,\bar{\theta})I & -N(z,\bar{\theta})I \\ \beta z^{-1}N(z,\bar{\theta})I & -\beta z^{-1}N(z,\bar{\theta})I \end{pmatrix}\begin{pmatrix} u \\ q \end{pmatrix}, \\ q &= \delta\theta(k)I\ p \end{aligned} \tag{13}$$

The time-invariant part of the controller is parameterised by $K(z) = Y(z)^{-1}X(z)$ and is computed by a convex optimisation problem to guarantee closed-loop stability for all the variations in the scheduling parameter $\theta(k)$ (see Algorithm 1).

B. Generalized model as LFR

After having "pulled out" $\delta\theta(k)$ from the LPV part of the controller and represent it as an LFR, the LTI plant model P_2 will be augmented with $\mathcal{N}$ and will be represented by an LFR. The augmented plant G^s maps q and the control inputs u to p and y_2 (the output of P_2) and is given by:

$$\begin{aligned} \begin{pmatrix} p \\ y_2 \end{pmatrix} &= \begin{pmatrix} G_{11}^s & G_{12}^s \\ G_{21}^s & G_{22}^s \end{pmatrix}\begin{pmatrix} q \\ u \end{pmatrix} \\ &= \begin{pmatrix} -\mathcal{N}_{22} & \mathcal{N}_{21} \\ -P_2\mathcal{N}_{12} & P_2\mathcal{N}_{11} \end{pmatrix}\begin{pmatrix} q \\ u \end{pmatrix} \end{aligned} \tag{14}$$

This augmented plant does not include the disturbance d and will be used to define a convex set of stabilizing controllers. The scheme representing the augmented system is given in Fig. 4.

Note that the time-varying filter ensures asymptotic attenuation of the disturbances. For the transitory phase, we do not consider the attenuation performance as the estimation of the scheduling parameter requires a certain time lapse for convergence. However, for nominal performance specifications, another augmented plant can be defined to constrain the effect

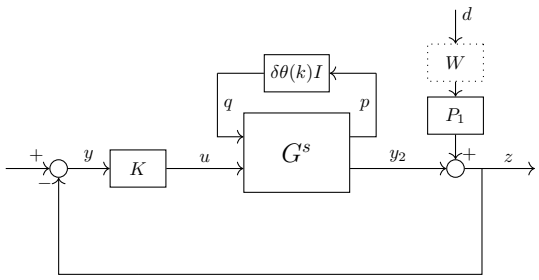

Fig. 4. Closed-loop scheme with the augmented system

of the external perturbation signal d on the performance channel z (see Fig. 4). The LFR of the corresponding augmented plant G^p is given by

$$\begin{pmatrix} z \\ y \end{pmatrix} = \begin{pmatrix} G^p_{11} & G^p_{12} \\ G^p_{21} & G^p_{22} \end{pmatrix} \begin{pmatrix} d \\ u \end{pmatrix} \tag{15}$$

$$= \begin{pmatrix} P_1 W & P_2 \mathcal{N}_{11} \\ -P_1 W & -P_2 \mathcal{N}_{11} \end{pmatrix} \begin{pmatrix} d \\ u \end{pmatrix}, \tag{16}$$

where W is a weighting factor which can be chosen according to the desired performance. A simple choice is to consider $\|T_{zd}\|_\infty < 1$ as the nominal performance and choose W as a constant to limit the amplification of the disturbances at all frequencies.

C. Controller Design

The stability for arbitrarily fast variation of the scheduling parameter shall be guaranteed using an IQC-based constraint.

A simplified solution for Π in accordance to (3), choosing $D = I$ and $E = 0$, is given by

$$\Pi_s = \begin{pmatrix} \eta^2 I & 0 \\ 0 & -I \end{pmatrix}. \tag{17}$$

When inserting (17) in (2), the obtained inequality can be simplified:

$$\begin{bmatrix} T_{pq}(e^{j\omega}) \\ I \end{bmatrix}^* \begin{pmatrix} \eta^2 I & 0 \\ 0 & -I \end{pmatrix} \begin{bmatrix} T_{pq}(e^{j\omega}) \\ I \end{bmatrix} \prec 0 \qquad \forall \omega \in \Omega$$

$$\Leftrightarrow \quad T^*_{pq}(e^{j\omega}) T_{pq}(e^{j\omega}) \prec \eta^{-2} I \qquad \forall \omega \in \Omega \tag{18}$$

This inequality has the same form as the constraint in (6) and can be converted to a set of LMIs in the same way as for the general LFT systems presented in Section II-C and be integrated into a feasibility problem as follows:

$$\begin{aligned} & \text{Find } K \\ \text{s.t.} \quad & T^*_{zd}(e^{j\omega}) T_{zd}(e^{j\omega}) \preceq I, \qquad \forall \omega \in \Omega \\ & T^*_{pq}(e^{j\omega}) T_{pq}(e^{j\omega}) \prec \eta^{-2} I, \quad \forall \omega \in \Omega \end{aligned} \tag{19}$$

A feasible but undesirable solution to this problem is the controller $K = 0$. To avoid this solution, a minimal steady-state gain $g_{\min}$ of K shall be imposed. A lower-bound constraint can be formulated as follows:

$$\begin{aligned} & K(e^{j\omega})|_{\omega=0} = Y^{-1}(e^{j\omega})|_{\omega=0} X(e^{j\omega})|_{\omega=0} \succ g_{\min} I \\ \Rightarrow \quad & X(1) - g_{\min} Y(1) \succ 0 \end{aligned} \tag{20}$$

Based on (19) and (20), we can now define an optimisation problem to maximize η. The objective is to compute a $K(z)$ which guarantees robust stability for all $\theta(k)$ satisfying $|\delta\theta(k)| \leq \eta$. The constraints in (19) can now be transformed into LMI in the form of (9) using the method presented in Section II-C.

The procedure to obtain the desired controller $K(z)$ is summarized in Algorithm 1. An iterative approach is proposed to reduce the conservatism related to the choice of the initial controller $K_c = 0$. At each new iteration, K_c is initialized with the optimal controller of the last iteration. The stopping criterion $\epsilon > 0$ should be sufficiently small such that the problem is feasible in the first iteration. The optimisation problems in this paper are formulated using frequency-domain constraints for all $\omega \in \Omega$. They correspond to convex semi-infinite programs (SIP) that cannot be solved with conventional solvers. A practical approach to solve such SIP is to sample the infinite number of constraints for the complete Ω at a large finite set of frequencies with a reasonable amount of frequency points $\Omega_f = \{\omega_1, \ldots, \omega_f\}$, although this does not theoretically guarantee that the constraints are met between the sampled frequencies. The scenario approach [28] can be used to obtain some probabilistic guarantee. Under some assumptions on the maximum error between the sampled plant model and the true system, the stability can be guaranteed using finite samples [29].

Algorithm 1 LPV control design algorithm

Require: $K_c = 0, \eta_0 = 0, \epsilon > 0, i = 1$

Require: $\eta_1 > \epsilon$

while $\eta_i - \eta_{i-1} > \epsilon$ **do**

- $\max\limits_{\eta_i, X, Y} \quad \eta_i$

s.t. $\begin{pmatrix} \eta_i^{-2} I - \Lambda & (\Phi^s G^s_{11} + X G^s_{21})^* \\ \star & \Phi^s (\Phi^s_c)^* + \Phi^s_c (\Phi^s)^* - \Phi^s_c (\Phi^s_c)^* \end{pmatrix} \succ 0,$

$\begin{pmatrix} I - \Lambda & (\Phi^p G^p_{11} + X G^p_{21})^* \\ \star & \Phi^p (\Phi^p_c)^* + \Phi^p_c (\Phi^p)^* - \Phi^p_c (\Phi^p_c)^* \end{pmatrix} \succ 0$

$\forall \omega \in \Omega_f,$

where $\Phi^p = (Y - X G^p_{22}) (G^p_{12})^{\mathsf{L}},$

$\Phi^s = (Y + X G^s_{22}) (G^s_{12})^{\mathsf{L}},$

$X(1) - g_{\min} Y(1) \succ 0,$

- $K_c = Y^{-1} X$
- Increment i

end while

The choice of Π_s as presented in (17) is conservative because the off-diagonal terms are set to zero. Hence, the achievable η is somewhat larger than the value obtained with Algorithm 1. Conservatism can be reduced using a fully parameterized Π given by 3. Algorithm 2 can be used after the completion of Algorithm 1 to obtain a stability guarantee for an interval bound $\eta_{\max}$ which is larger than η_n obtained from the Algorithm 1 after n iterations. Algorithm 2 can be solved using a bisection approach or by iteratively increasing

the value of $\eta_{\max}$ and checking the feasibility of the problem.

Algorithm 2 Stability analysis of final controller

$$\begin{aligned}
&\max_{\Pi,\eta_{\max}} \quad \eta_{\max} \\
\text{s.t.} &\begin{bmatrix} T_{pq}(e^{j\omega}) \\ I \end{bmatrix}^* \Pi \begin{bmatrix} T_{pq}^*(e^{j\omega}) \\ I \end{bmatrix} \prec 0 \qquad \forall \omega \in \Omega_f, \\
&\begin{bmatrix} I \\ \eta_{\max} I \end{bmatrix}^* \Pi \begin{bmatrix} I \\ \eta_{\max} I \end{bmatrix} \succ 0, \\
&D = D^T \succ 0, \quad E = -E^T
\end{aligned}$$

D. Controller structure for multi-harmonic rejection

In presence of a sinusoidal perturbation signal containing n harmonic frequencies $\rho(k) = [\rho_1, \rho_2, ..., \rho_n]$, a sequence of time-varying filters stacked in parallel can be defined as:

$$N\left(z, \theta_1(k), ..., \theta_n(k)\right) = \sum_{i=1}^{n} N(z, \theta_i(k)), \tag{22}$$

where $\theta_i(k) = -2\cos\left(T_s \rho_i(k)\right)$. In a similar way the time-varying filter can be represented by an LFR including an LTI filter and a time-varying block as:

$$q = \begin{pmatrix} \delta\theta_1(k) I & \mathbf{0} & \mathbf{0} & \mathbf{0} \\ \mathbf{0} & \delta\theta_2(k) I & \mathbf{0} & \mathbf{0} \\ \mathbf{0} & \mathbf{0} & \ddots & \mathbf{0} \\ \mathbf{0} & \mathbf{0} & \mathbf{0} & \delta\theta_n(k) I \end{pmatrix} p \tag{23}$$

Similar to the development of (14), a generalized plant $G_n^p(e^{j\omega})$ can be computed by defining $\theta_i(k) = \bar{\theta}_i + \delta\theta_i(k)$ (see Eq. 21). The control system architecture for the multiharmonic case is schemetically presented in Fig. 5.

IV. Experimental Results

A. Hybrid micro-vibration damping platform (MIVIDA)

Novel high-precision optical instruments designed for Earth observation missions demand an exceptionally high pointing accuracy. These line-of-sight stability requirements constrain the admissible level of mechanical vibration that can occur onboard a spacecraft. Micro-vibrations are caused by primary satellite systems such as reaction wheels, thrusters, cryocoolers, or solar array drive mechanisms, and have the potential to significantly degrade the performance of the sensitive payloads.

A hybrid active-passive micro-vibration damping platform (MIVIDA), aimed at mitigating micro-vibrations and isolating the sensitive optical payload from external disturbances, was developed at CSEM. The objective is to study in a more general context the stabilisation of sensitive active payloads from multiple unknown external perturbations. The modular platform consists of an adjustable number of passive dampers, a set of proof mass actuators (PMA) creating a 6 degree of freedom (DoF) force tensor, and a payload interface allowing to accommodate various types of sensitive instruments. The platform utilises accelerometer measurements in close proximity to the payload to actively reject disturbances from the satellite body. These external perturbations are generated using an external inertial shaker. An image of the system is shown in Fig. 6. All experimental tests with the platform are carried out at the Microvibration Characterisation Facility at CSEM in Neuchâtel, Switzerland [30].

B. Scheduling parameter estimation

The scheduling parameter is updated by estimating the main harmonic frequency of the perturbation. As the perturbation signal d cannot be measured directly, an estimation of the harmonic frequency is calculated based on a sliding discrete Fourier transform (SDFT) on the output signal y. The SDFT is implemented using the algorithm presented in [31]. The discrete Fourier transform (DFT) at instant k for an N length window is given by

$$\mathcal{Y}_n(k) = \sum_{i=0}^{N-1} y(k-i) e^{-\left(\frac{j2\pi(k-i)n}{N}\right)},$$

where $0 \leq n \leq N-1$ designates the n^{th} bin of the N-point DFT. The DFT can be computed recursively using the SDFT algorithm. Essentially, the SDFT algorithm arises from the fact that for two successive times, the sequences $y(k-1)$ and $y(k)$ contain mainly identical elements. The recursive update step of the SDFT at time k can therefore be expressed by

$$\mathcal{Y}_n(k) = e^{\frac{j2\pi n}{N}} \big(\mathcal{Y}_n(k-1) + y(k) - y(k-N)\big).$$

Based on the m highest peaks present in $\mathcal{Y}_n(k)$, m harmonic frequencies $\rho_i, i = 1, ..., m$ are identified in real time. The values of ρ_i are then used to update the value of $\theta_i(k) = -2\cos T_s \rho_i(k)$.

$$\begin{pmatrix} p_1 \\ \vdots \\ p_i \\ \vdots \\ p_n \\ y \end{pmatrix} = \begin{pmatrix} -\beta z^{-1} N(\bar{\theta}_1) I & & & \mathbf{0}_{1\times(n-1)} & \beta z^{-1} N(\bar{\theta}_1) I \\ & & & \vdots & \\ \mathbf{0}_{1\times(i-1)} & -\beta z^{-1} N(\bar{\theta}_i) I & & \mathbf{0}_{1\times(n-i)} & \beta z^{-1} N(\bar{\theta}_i) I \\ & & & \vdots & \\ & & \mathbf{0}_{1\times(n-1)} & -\beta z^{-1} N(\bar{\theta}_n) I & \beta z^{-1} N(\bar{\theta}_n) I \\ P_2 N(\bar{\theta}_1) I & \dots & P_2 N(\bar{\theta}_i) I \quad \dots & P_2 N(\bar{\theta}_n) I & -P_2 \sum_{j=1}^{n} N(\bar{\theta}_j) I \end{pmatrix} \begin{pmatrix} q_1 \\ \vdots \\ q_i \\ \vdots \\ q_n \\ u \end{pmatrix}, \tag{21}$$

$$u = Ky$$

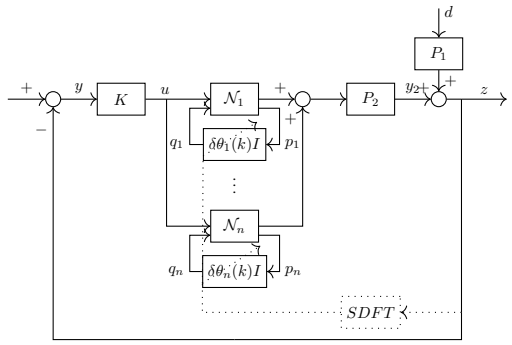

Fig. 5. Control scheme with $\mathcal{N}_1, ..., \mathcal{N}_n$ for the multi-harmonic case

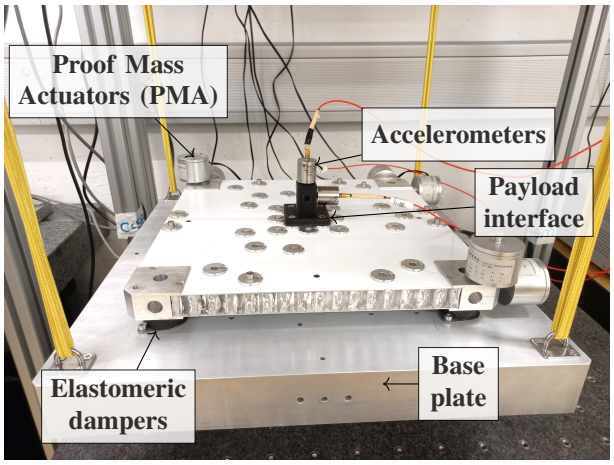

Fig. 6. Hybrid micro-vibration damping platform MIVIDA developed at CSEM, Switzerland

C. Single harmonic rejection validation on MIVIDA

The here presented method is used to design a controller for the MIVIDA platform allowing to adaptively reject sinusoidal disturbances. A system identification experiment is carried out to compute an FRF matrix directly from experimental data using a frequency grid with 1000 points and a sampling frequency of 1 kHz. For the control design, a controller order of 40 is chosen. The controller order is determined by comparing the resulting η for several controllers with different orders. For the final controller, the smallest possible order that achieves the highest value of η is chosen. The center frequency $\bar{\rho}$ is set to 60 Hz, ϵ to 0.1, $g_{\min}$ to 1 and the damping parameter β for $N(z, \theta(k))$ is chosen as $\beta = 0.999$. This is the highest value of β leading to a feasible solution for this application. The performance weighting factor W is chosen as $W = -20I$ dB to limit the infinity norm of the sensitivity function. The identified FRF matrices $P_1(e^{j\omega})$ and $P_2(e^{j\omega})$ together with the computed sensitivity function $S(e^{j\omega}, \theta) = \left(I + P_2(e^{j\omega})K_N(e^{j\omega}, \theta)\right)^{-1}$ for different values of θ are presented in Fig. 7. It can be observed that the disturbance frequency is attenuated around 35 to 50 dB along the three axes. The obtained controller guarantees stability for a value of $\delta\rho_{\max} = 16$ Hz. This is the resulting value obtained with Algorithm 2 using a fully parameterized Π. The value obtained after the last iteration with Algorithm 1 is $\delta\rho_{\max} = 10$ Hz. For comparison, an LTI controller with $\beta = 1$ was computed. With this controller, a 30 dB attenuation can be obtained for a value of only $\delta\rho = 0.8$ Hz.

	Attenuation Performance (dB)		
	X-axis	Y-axis	Z-axis
$\rho(k) = \bar{\rho} = 60$ Hz	50.40 (48.05)	44.07 (51.36)	36.06 (46.37)
$\rho(k) = \bar{\rho} - \delta\rho_{\max} = 44$ Hz	25.87 (24.60)	24.31 (27.46)	15.30 (17.56)
$\rho(k) = \bar{\rho} + \delta\rho_{\max} = 76$ Hz	38.38 (41.72)	10.10 (18.26)	27.13 (33.15)

TABLE I

ATTENUATION PERFORMANCE ACHIEVED WITH THE IQC-BASED LPV CONTROLLER AT DIFFERENT VALUES OF $\rho(k)$, THE VALUES IN THE PARENTHESIS INDICATE THE CALCULATED ATTENUATION PERFORMANCE FROM THE COMPUTED SENSITIVITY FUNCTION $S(\theta(k))$ (SEE FIG. 7)

A dSpace rapid prototyping platform is used as real-time control system at a sampling frequency of 1 kHz. Two individual power amplifiers generate the power supply and the analog input and output signals for the PMA and the accelerometers respectively. A third control module is used for the command of the external inertial shaker. For performance evaluation, a sinusoidal perturbation along the x-axis is injected with this shaker. In Fig. 8, the measured accelerations along the three axes in open- and closed-loop are shown. The harmonic frequency $\rho(k)$ of the sinusoidal perturbation is shifted in the interval of $\rho(k) \in [44, 76]$ Hz increasing the frequency by 2 Hz every 5 seconds. Table 1 shows the obtained attenuation values for different values of $\rho(k)$. The difference between the attenuation computed using the sensitivity function and the experimental results comes from the magnitude of the primary path model $P_1(e^{j\omega})$ at the disturbance frequencies. Furthermore, the actual limit of stability when increasing the value of $\delta\rho_{\max}$ was assessed. When injecting a sinusoidal perturbation with $\rho(k) = 37$ Hz, the closed-loop system becomes unstable. Hence, there is some margin in the stability limit determined at $\delta\rho_{\max} = 16$ Hz while the experimentally determined value is at approximately $\delta\rho_{\max} = 22$ Hz.

An additional test has been performed to assess the closed-loop stability for a fast variation of the scheduling parameter. During that test, the harmonic frequency $\rho(k)$ of the sinusoidal perturbation is increased by 1 Hz every 100 milliseconds in the interval of $\rho(k) \in [36, 84]$. From Fig. 9, it can be observed that the stability is still guaranteed in closed-loop. Note that the attenuation performance cannot be achieved in that case as the estimation of the disturbance frequency leads to wrong results. The update period of the SDFT needs to be at least 300 milliseconds to obtain a correct estimation. However, the stability of the closed-loop is still guaranteed even if the estimated disturbance frequency has a large error with respect to the true one.

D. Multi-harmonic rejection validation on MIVIDA

Using the method presented in Section III-D, a controller containing two time-varying filters in parallel was computed to be applied on MIVIDA. The center frequency $\bar{\rho}_1$ is chosen

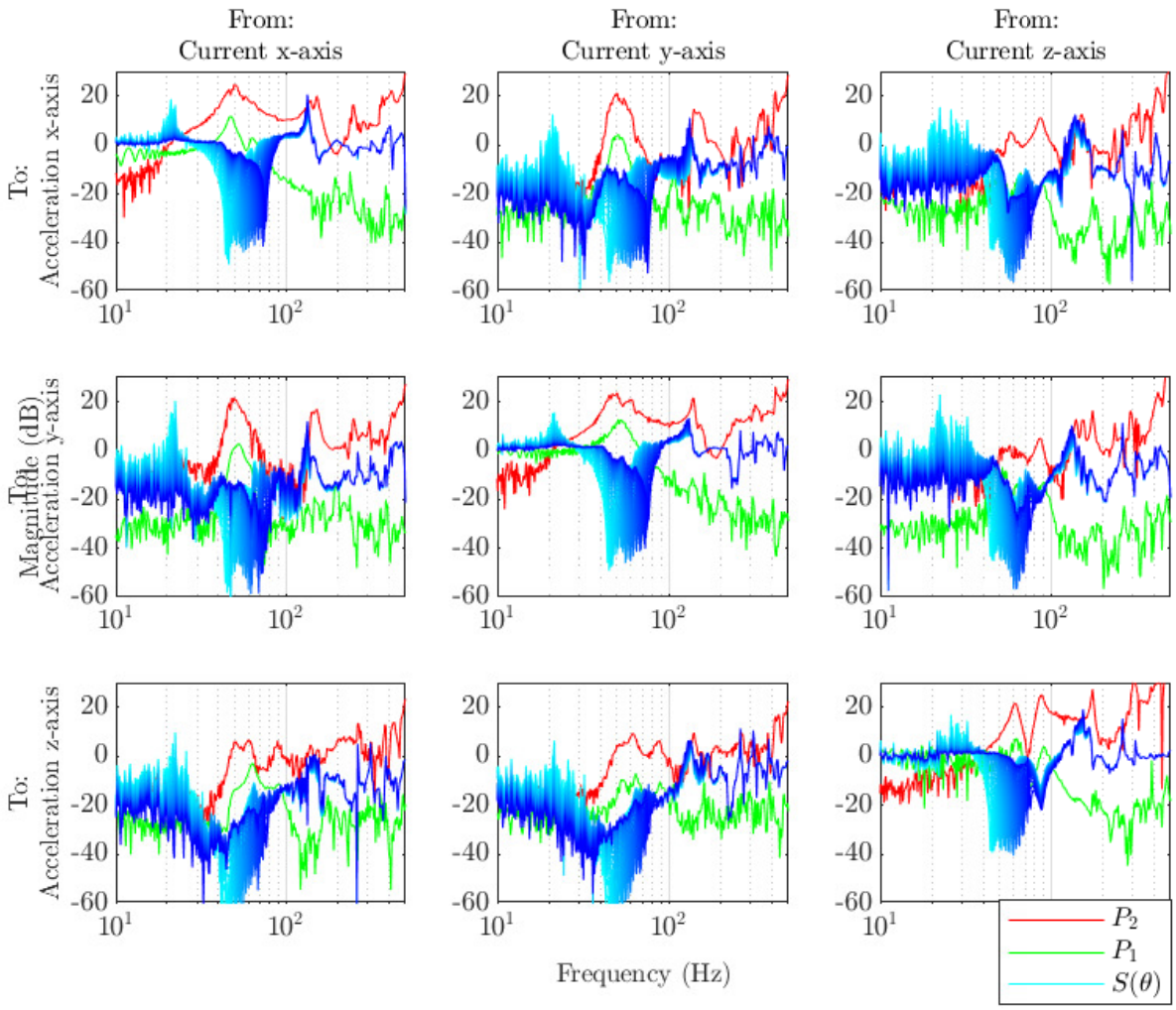

Fig. 7. Closed-loop sensitivity functions $S(e^{j\omega}, \theta)$ for different values of θ (from light blue to dark blue) and FRF matrix of perturbation model $P_1(e^{j\omega})$ and of plant model $P_2(e^{j\omega})$

at 50 Hz and $\bar{\rho}_2 = 70$ Hz with $\epsilon = 0.1$,$\beta = 0.999$ and a controller order of 60. The obtained controller guarantees stability for a value of $\delta\rho_{\max} = 5$ Hz. A test injecting a sinusoidal perturbation containing two harmonics was performed. The resulting attenuation performance is presented in Table IV-D. A disturbance attenuation of up to 22.60 dB can be experimentally achieved for the central frequency $\bar{\rho}_1$. However, the achieved performance is significantly smaller for other values of ρ_1 and ρ_2 and for other axes. when looking at P_2 (see Fig. 7), one can see that the overall magnitude at $\bar{\rho}_2$ is smaller compared to the one at $\bar{\rho}_1$. The signal-to-noise ratio of the accelerometers is therefore smaller at $\bar{\rho}_2$ leading to smaller attenuation performances at higher frequencies. Furthermore, with the given controller structure it is difficult to achieve acceptable performance for multiharmonic rejection due to the parametrization of $N(z, \theta(k))$ with its limited damping adjustment possibilities and due to the waterbed effect. To improve the attenuation performance, a more flexible LPV control structure $K(\theta)$ without fixed parametrization $N(z, \theta(k))$ can be used. In addition, it is possible to use a fully parametrized Π as given by (3) also for control synthesis. Such a development is part of on-going work.

		Attenuation Performance (dB)		
ρ_1 (Hz)	ρ_2 (Hz)	X-axis	Y-axis	Z-axis
50 ($= \bar{\rho}_1$)		18.56	20.56	20.69
	70 ($= \bar{\rho}_2$)	18.51	11.81	17.20
50		16.04	18.37	16.22
	65	12.31	12.04	9.48
50		18.42	20.43	20.70
	75	18.90	2.28	18.38
45		20.68	14.24	19.41
	65	19.42	17.24	22.30
45		20.54	13.58	19.37
	70	19.00	9.38	21.02
45		20.54	13.42	19.53
	75	19.26	-3.72	21.62
55		19.19	19.91	22.24
	65	19.40	17.13	22.60
55		19.30	19.69	22.49
	70	18.79	10.40	20.98
55		16.30	16.70	19.54
	75	16.46	1.54	18.45

TABLE II
ATTENUATION PERFORMANCE ACHIEVED WITH THE LPV CONTROLLER FOR DOUBLE HARMONIC REJECTION

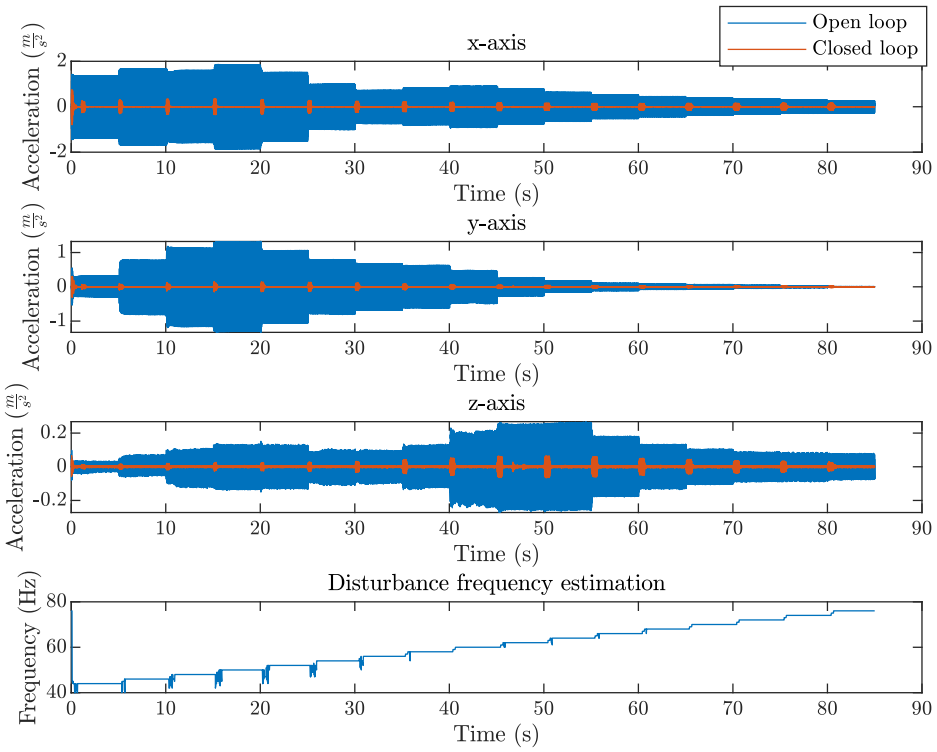

Fig. 8. Closed-loop attenuation test

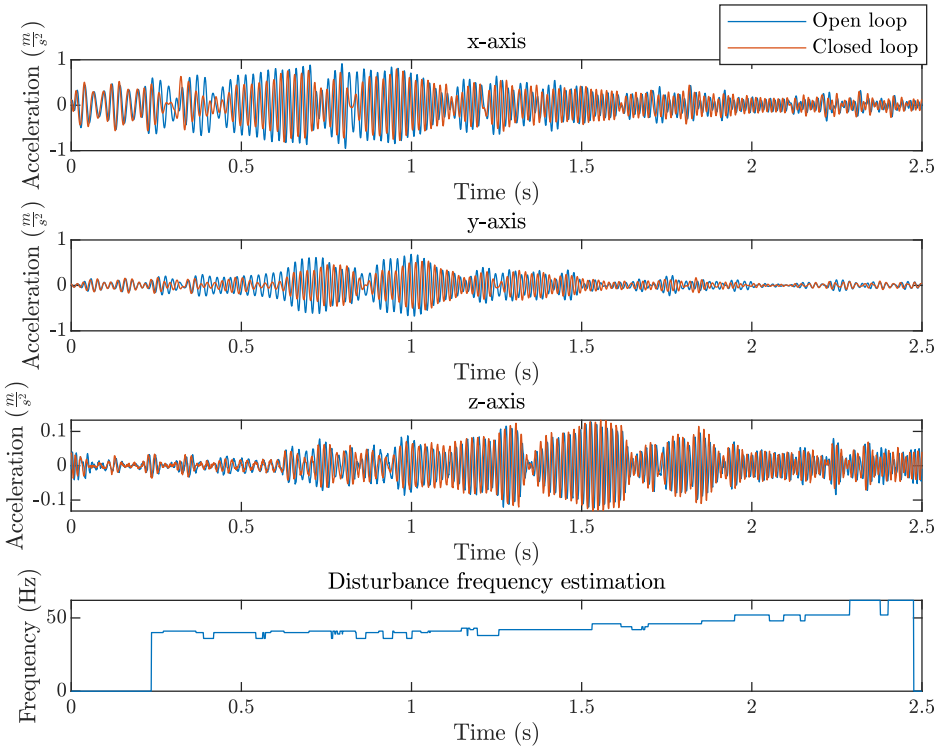

Fig. 9. Fast parameter variation test

V. Conclusions

Given an FRF matrix of an LTI-MIMO system, an LPV controller is computed for adaptive rejection of an unknown external perturbation signal. Using an IQC describing a time-varying real scalar, an equivalent LMI is computed which is included in a two-step iterative control design algorithm. This method ensures the stability of the controller for arbitrarily fast variations of the scheduling parameters lying in a bounded interval. An LPV controller was designed for the hybrid micro-vibration damping platform using the proposed method. The resulting controller achieves a disturbance attenuation of up to 50.40 dB in the case of single harmonic rejection and up to 22.60 dB for multi-harmonic rejection while guaranteeing stability for scheduling parameters with an arbitrarily fast variation.

References

[1] H. E. Tseng and D. Hrovat, "State of the art survey: active and semi-active suspension control," *Vehicle System Dynamics*, vol. 53, no. 7, pp. 1034–1062, 2015. [Online]. Available: http://www.tandfonline.com/doi/full/10.1080/00423114.2015.1037313

[2] Q. Zheng, L. Dong, D. H. Lee, and Z. Gao, "Active disturbance rejection control for MEMS gyroscopes," *IEEE Transactions on Control Systems Technology*, 2009.

[3] R. Fareh, S. Khadraoui, M. Y. Abdallah, M. Baziyad, and M. Bettayeb, "Active disturbance rejection control for robotic systems: A review," *Mechatronics*, vol. 80, p. 102671, 2021. [Online]. Available: https://linkinghub.elsevier.com/retrieve/pii/S0957415821001392

[4] V. Nguyen, J. Johnson, and S. Melkote, "Active vibration suppression in robotic milling using optimal control," *International Journal of Machine Tools and Manufacture*, vol. 152, 2020. [Online]. Available: https://linkinghub.elsevier.com/retrieve/pii/S0890695519312623

[5] T.-B. Airimitoaie, I. D. Landau, R. Melendez, and L. Dugard, "Algorithms for adaptive feedforward noise attenuation—a unified approach and experimental evaluation," *IEEE Transactions on Control Systems Technology*, vol. 29, no. 5, pp. 1850–1862, 2021. [Online]. Available: https://ieeexplore.ieee.org/document/9203846/

[6] P. Ballesteros and C. Bohn, "Disturbance rejection through LPV gain-scheduling control with application to active noise cancellation," *IFAC Proceedings Volumes*, vol. 44, no. 1, pp. 7897–7902. [Online]. Available: https://linkinghub.elsevier.com/retrieve/pii/S1474667016448779

[7] C. Bohn, A. Cortabarria, V. Härtel, and K. Kowalczyk, "Disturbance-observer-based active control of engine-induced vibrations in automotive vehicles," in *Smart Structures and Materials 2003: Modeling, Signal Processing, and Control*, R. C. Smith, Ed., vol. 5049, International Society for Optics and Photonics. SPIE, 2003, pp. 565 – 576. [Online]. Available: https://doi.org/10.1117/12.482709

[8] C. Kinney and R. De Callafon, "An adaptive internal model-based controller for periodic disturbance rejection," *IFAC Proceedings Volumes*, vol. 39, no. 1, pp. 273–278. [Online]. Available: https://linkinghub.elsevier.com/retrieve/pii/S1474667015352745

[9] I. D. Landau, A. Castellanos Silva, T.-B. Airimitoaie, G. Buche, and M. Noe¨, "Benchmark on adaptive regulation—rejection of unknown/time-varying multiple narrow band disturbances," vol. 19, no. 4, pp. 237–252. [Online]. Available: https://linkinghub.elsevier.com/retrieve/pii/S0947358013000721

[10] X. Chen and M. Tomizuka, "Selective model inversion and adaptive disturbance observer for rejection of time-varying vibrations on an active suspension," in *2013 European Control Conference (ECC)*. IEEE, pp. 2897–2903. [Online]. Available: https://ieeexplore.ieee.org/document/6669759/

[11] A. Karimi and Z. Emedi, "H-inf gain-scheduled controller design for rejection of time-varying narrow-band disturbances applied to a benchmark problem," *European Journal of Control*, vol. 19, no. 4, pp. 279–288. [Online]. Available: https://linkinghub.elsevier.com/retrieve/pii/S0947358013000757

[12] B. Vau and I. D. Landau, "Adaptive rejection of narrow-band disturbances in the presence of plant uncertainties—a dual youla–kucera approach," *Automatica*, vol. 129, p. 109618. [Online]. Available: https://linkinghub.elsevier.com/retrieve/pii/S0005109821001382

[13] A. Karimi and C. Kammer, "A data-driven approach to robust control of multivariable systems by convex optimization," *Automatica*, vol. 85, pp. 227–233, Nov. 2017.

[14] S. S. Madani and A. Karimi, "Data-Driven Passivity-Based Current Controller Design for Power-Electronic Converters of Traction Systems," in *Proceedings of the IEEE Conference on Decision and Control*, Jeju Island, Republic of Korea, Dec. 2020, pp. 842–847.

[15] S. S. Madani, C. Kammer, and A. Karimi, "Data-Driven Distributed Combined Primary and Secondary Control in Microgrids," *IEEE Transactions on Control Systems Technology*, vol. 29, no. 3, pp. 1340–1347, May 2021.

[16] S. S. Madani and A. Karimi, "Data-driven LPV controller design for islanded microgrids," *IFAC-PapersOnLine*, vol. 54, no. 7, pp. 433–438, 2021. [Online]. Available: https://linkinghub.elsevier.com/retrieve/pii/S2405896321011721

[17] P. Schuchert and A. Karimi, "Frequency-domain data-driven position-dependent controller synthesis for cartesian robots," *IEEE Transactions on Control Systems Technology*, vol. 31, no. 4, pp. 1855–1866, 2023. [Online]. Available: https://ieeexplore.ieee.org/document/10081199/

[18] A. Megretski and A. Rantzer, "System analysis via integral quadratic constraints," *IEEE Transactions on Automatic Control*, vol. 42, no. 6, pp. 819–830, Jun. 1997.

[19] J. Veenman, C. W. Scherer, and H. Köroğlu, "Robust stability and performance analysis based on integral quadratic constraints," *European Journal of Control*, vol. 31, pp. 1–32, Sep. 2016.

[20] S. Michalowsky, C. Scherer, and C. Ebenbauer, "Robust and structure exploiting optimisation algorithms: An integral quadratic constraint approach," *International Journal of Control*, vol. 94, no. 11, pp. 2956–2979, 2021.

[21] J. Veenman, C. W. Scherer, C. Ardura, S. Bennani, V. Preda, and B. Girouart, "IQClab: A new IQC based toolbox for robustness analysis and control design," *IFAC-PapersOnLine*, vol. 54, no. 8, pp. 69–74, Jan. 2021.

[22] A. Koch, J. Berberich, J. Köhler, and F. Allgöwer, "Determining optimal input–output properties: A data-driven approach," *Automatica*, vol. 134, p. 109906, Dec. 2021.

[23] T. Bloemers, T. Oomen, and R. Toth, "Frequency Response Data-Driven LPV Controller Synthesis for MIMO Systems," *IEEE Control Systems Letters*, vol. 6, pp. 2264–2269, 2022.

[24] T. Bloemers, T. Oomen, and R. Tóth, "Frequency Response Data-Based LPV Controller Synthesis Applied to a Control Moment Gyroscope," *IEEE Transactions on Control Systems Technology*, vol. 30, no. 6, pp. 2734–2742, Nov. 2022.

[25] J. M. Fry, D. Abou Jaoude, and M. Farhood, "Robustness analysis of uncertain time-varying systems using integral quadratic constraints with time-varying multipliers," vol. 31, no. 3, pp. 733–758. [Online]. Available: https://onlinelibrary.wiley.com/doi/10.1002/rnc.5299

[26] R. Pintelon and J. Schoukens, *System Identification: A Frequency Domain Approach*, 2nd ed. John Wiley & Sons, Ltd, 2012.

[27] P. Schuchert, V. Gupta, and A. Karimi, "Data-driven fixed-structure frequency-based $\mathcal{H}_2$ and $\mathcal{H}_\infty$ controller design," *Automatica*, vol. 160, no. 111398, 2024. [Online]. Available: https://doi.org/10.1016/j.automatica.2023.111398

[28] G. Calafiore and M. Campi, "The Scenario Approach to Robust Control Design," *IEEE Transactions on Automatic Control*, vol. 51, no. 5, pp. 742–753, May 2006.

[29] P. Schuchert and A. Karimi, "Robust Data-Driven Controller Design with Finite Frequency Samples," 2024. [Online]. Available: https://infoscience.epfl.ch/record/309148

[30] E. Onillon, T. Adam, G. B. Gallego, and E. Klauser, "CSEM micro-vibration characterisation facility description and validation," in *European Space Mechanisms and Tribology Symposium (ESMATS)*, Warsaw, Poland, Sep. 2021.

[31] R. Lyons, "dsp tips & tricks - the sliding DFT," *IEEE Signal Processing Magazine*, vol. 20, no. 2, pp. 74–80, 2003. [Online]. Available: http://ieeexplore.ieee.org/document/1184347/